Letter

Magnon-mediated topological superconductivity in a quantum wire

Florinda Viñas Boström [1,2,*] and Emil Viñas Boström [3,4,†]

[1]*Institut für Mathematische Physik, Technische Universität Braunschweig, D-38106 Braunschweig, Germany*

[2]*Division of Solid State Physics and NanoLund, Lund University, Box 118, S-221 00 Lund, Sweden*

[3]*Nano-Bio Spectroscopy Group, Departamento de Física de Materiales, Universidad del País Vasco, 20018 San Sebastian, Spain*

[4]*Max Planck Institute for the Structure and Dynamics of Matter, Luruper Chaussee 149, 22761 Hamburg, Germany*

(Received 5 December 2023; revised 28 March 2024; accepted 2 May 2024; published 16 May 2024)

Many emergent phases of matter stem from the intertwined dynamics of quasiparticles. Here we show that a topological superconducting phase emerges as the result of interactions between electrons and magnons in a quantum wire and a helical magnet. The magnon-mediated interaction favors triplet superconductivity over a large magnetic phase space region, and stabilizes topological superconductivity over an extended region of chemical potentials. The superconducting gap depends exponentially on the spin-electron coupling, allowing it to be enhanced through material engineering techniques.

DOI: 10.1103/PhysRevResearch.6.L022042

The intertwined dynamics of collective excitations underlies many diverse phenomena observed in condensed matter systems. A prominent example where such interactions play a key role is in the effective phonon-mediated attraction between electrons, responsible for the superconducting instability of simple metals at low temperatures [1]. Other emergent phases driven by quasiparticle interactions include the spontaneous electric polarization of ferroelectric and multiferroic materials in response to lattice distortions [2,3], the binding between electrons and holes and their possible subsequent condensation into an excitonic insulator [4,5], and the stabilization of fractional quantum Hall states through electron-electron interactions [6].

Many emergent phases themselves give rise to quasiparticles with potentially unconventional properties. In particular, the excitations of topologically ordered systems [7–9] such as fractional quantum Hall systems, quantum spin liquids, and topological superconductors [10–14], termed anyons [15,16], have garnered much interest due to their promise in realizing fault-tolerant quantum computing. In particular, the subclass known as non-Abelian anyons allow for information to be nonlocally encoded and processed in the braiding patterns of the anyon world lines [8,9]. In topological superconductors, non-Abelian anyons may appear in vortex cores of chiral two-dimensional superconductors [17–23], or at the ends of one-dimensional (1D) quantum wires [24–39]. However, to stabilize a topological superconducting phase, the pairing needs to be mediated by quasiparticles carrying an intrinsic spin structure that favors spin triplet over spin singlet pairing.

As a prominent example, magnon-mediated topological superconductivity has recently been proposed for two-dimensional systems with noncollinear magnetic order, such as skyrmion crystals and helical magnets in proximity to a two-dimensional normal metal surface [40–42]. However, since the majority of experimental studies on topological superconductivity is concerned with one-dimensional structures, identifying criteria for realizing magnon-mediated topological superconductivity in one dimension is of key importance. Indeed, both the superconducting and topological phenomenology is qualitatively different in one and two dimensions, stemming in large part from the different symmetry requirements necessary to realize a nontrivial topology in different dimensions [43–45]. In particular, to stabilize topological superconductivity in 2D it is necessary to obtain a time-reversal symmetric and fully gapped superconducting state, while in 1D systems a topological superconducting phase is realized by breaking time-reversal symmetry (thereby realizing an effective single-band regime), while simultaneously stabilizing triplet pairing. As will be demonstrated below, both these conditions are satisfied by the dynamical coupling between itinerant electrons and the magnons of a helical magnet, away from the collinear ferromagnetic and antiferromagnetic limits.

Specifically, we here investigate superconductivity resulting from the coupling between a quantum wire and a helical magnet (see Fig. 1). The magnons of the helical magnet mediate an effective attraction between electrons of arbitrary spin projection, thereby stabilizing unconventional triplet superconductivity over a large region of phase space. The noncollinear magnetic order induces an effective spin-orbit coupling (SOC) and Zeeman field among the electrons, that allows to realize an effective single-band regime over a finite range of chemical potentials. Within the single-band regime, the system enters a topological phase, with unpaired Majorana bound states at each end of the wire. Crucially, both the size

*florinda.vinas_bostrom@ftf.lth.se
†emil.bostrom@mpsd.mpg.de

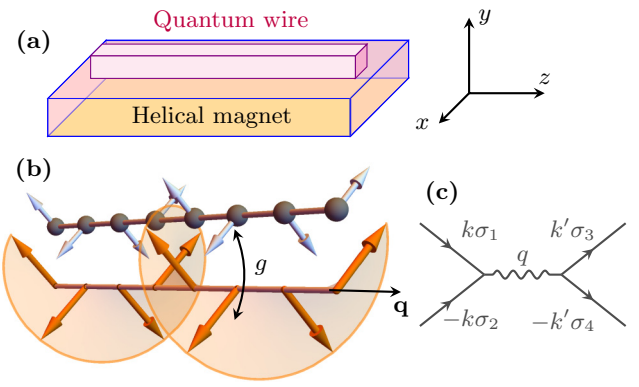

FIG. 1. Principles of magnon-mediated superconductivity. (a) Experimental setup with a quantum wire in proximity to a helical magnet. (b) The helical magnetic order (orange arrows) induces an effective spin-orbit interaction and Zeeman splitting of the electronic bands via the spin-electron coupling g. Magnon fluctuations around the equilibrium magnetic order provide an effective attractive interaction among the electrons (blue arrows). (c) Due to the noncollinear magnetic structure, magnon fluctuations mediate scattering between electrons with arbitrary spin projections σ_i.

of the effective single-band regime and the superconducting gap are increasing functions of the spin-electron coupling g. Our proposal thereby identifies quantum wires in proximity to helical magnets as a promising platform to realize topological superconductivity, without the need to proximitize the wire to a conventional superconductor. It also showcases the power of utilizing quasiparticle interactions to realize unconventional forms of matter.

To investigate magnon-mediated superconductivity in a quantum wire, we consider an interacting system of spins and electrons described by the lattice Hamiltonian

$$H = -t\sum_{\langle ij\rangle\sigma}\hat{c}^\dagger_{i\sigma}\hat{c}_{j\sigma} - J\sum_{\langle ij\rangle}\hat{\mathbf{S}}_i\cdot\hat{\mathbf{S}}_j - \sum_{\langle ij\rangle}\mathbf{D}_{ij}\cdot(\hat{\mathbf{S}}_i\times\hat{\mathbf{S}}_j) - g\sum_i\hat{\mathbf{s}}_i\cdot\hat{\mathbf{S}}_i. \quad (1)$$

Here $\hat{c}_{i\sigma}$ destroys an electron at site i and of spin projection σ, and $\hat{\mathbf{S}}_i$ is the spin operator at site i for a spin of magnitude S. The parameters t, J, and $\mathbf{D}$ respectively determine the nearest-neighbor electronic hopping amplitude, the exchange interaction, and the antisymmetric Dzyaloshinskii-Moriya interaction (DMI). The spins and electrons interact via a local spin-electron coupling of strength g, and the electronic spin operator is defined by $\hat{\mathbf{s}}_i = \sum_{\sigma\sigma'}\hat{c}^\dagger_{i\sigma}\boldsymbol{\tau}_{\sigma\sigma'}\hat{c}_{i\sigma'}$, with $\boldsymbol{\tau}$ the Pauli matrix vector.

The competition between exchange and DMI stabilizes a helical magnetic order, characterized by a propagation vector $\mathbf{q}$ and a vector $\hat{\mathbf{n}}$ defining the plane of polarization. Specifically, the magnitude of the spiral momentum is given by $\tan q = D/J$, while the directions of the momentum and polarization vectors are determined by the normalized DMI vector $\hat{\mathbf{D}}$. Here we consider a DMI such that the spiral momentum $\mathbf{q}$ lies along the wire axis $\hat{\mathbf{z}}$, and with $\hat{\mathbf{n}}$ parallel to $\mathbf{q}$ (see Fig. 1). The equilibrium spin texture is then a spin helix, and can be written as $\mathbf{S}_i = \cos(\mathbf{q}\cdot\mathbf{r}_i)\mathbf{e}_1 + \sin(\mathbf{q}\cdot\mathbf{r}_i)\mathbf{e}_2$, where the vectors $\mathbf{e}_\alpha$ and $\hat{\mathbf{n}}$ define a right-handed orthonormal system (see the Supplemental Material, SM [46]).

In the following the magnetic texture is assumed to be commensurate with the electronic lattice, such that the spin spiral is periodic over a distance La, where L is an integer and a is the electronic lattice parameter. To describe fluctuations around the equilibrium order, the spin operators $\hat{\mathbf{S}}_i$ are expressed in terms of a set of bosonic operators by performing a Holstein-Primakoff expansion around the local spin axis $\mathbf{S}_i$ (see the SM [46]). This results in a diagonal magnon Hamiltonian $H_m = \sum_{np}\Omega_{np}\alpha^\dagger_{np}\alpha_{np}$, where Ω_{np} is the energy of a magnon with momentum p in band n. The momentum runs over the magnetic Brillouin zone $[-\pi/La, \pi/La]$, and the number of magnon bands is L.

There are two main effects of the spin spiral on the electronic structure: First, the coupling to the equilibrium magnetic structure $\mathbf{S}_i$ induces an effective SOC and Zeeman splitting of the electronic bands [see Fig. 2(a)]. Second, the coupling to magnon fluctuations around the helical configuration generates an effective attractive interaction among the electrons, which ultimately leads to superconductivity. The effect of the static spin spiral can be exactly accounted for, by diagonalizing the electronic subsystem in presence of the spiral $\mathbf{S}_i$ (see the SM [46] and Ref. [47]), and results in the electron Hamiltonian $H_e = \sum_{k\tau}\epsilon_{k\tau}d^\dagger_{k\tau}d_{k\tau}$. Here τ denotes the electronic bands, and the momentum runs over the electronic Brillouin zone $[-\pi/a, \pi/a]$. The spiral shifts the minima of the originally spin-degenerate bands to $\pm q/2$ [Fig. 2(a)], thereby inducing an effective Rashba SOC. This shift is independent of the value of g, and is set for any finite g by the momentum of the spin spiral. In addition, the coupling opens a gap of size $\Delta_b = 2gS$ at $k = 0$ and $k = \pm\pi/a$, acting like an effective Zeeman field. Together these effects realize an effective single-band regime for chemical potentials inside the gap. The static effects of our model have been considered within the context of so-called Yu-Shiba-Rusinov chains [48], which give rise to a similar induced spin-orbit coupling and Zeeman splitting of the electronic bands. However, these earlier treatments neglect the dynamical effects of the spin-electron interaction, which here gives rise to an intrinsic triplet superconductivity.

The electron-magnon interaction is found by expressing the spin-electron coupling [the last term in Eq. (1)] in terms of the magnon and band electron operators. Due to the noncollinear structure of the spin spiral, the coupling has a nontrivial spin structure [see Fig. 1(c)], and in general gives rise to magnon-mediated scattering between electrons with arbitrary spin projections. An effective electron-electron interaction is obtained by integrating out the magnons within a finite-temperature functional integral formulation (see the SM [46]). The effective interaction $U^{\tau_3\tau_4}_{\tau_1\tau_2}(k,k')$ implicitly depends on the magnetic structure via the spin-electron coupling g, the spiral momentum q, and the transformation matrices used to diagonalize the magnon and electron subsystems. In the static limit the superconducting gap $\Delta^{\tau\tau'}_k$ is determined via the linearized gap equation

$$\Delta^{\tau_1\tau_2}_k = \sum_{k'\tau_3\tau_4}U^{\tau_3\tau_4}_{\tau_1\tau_2}(k,k')\left(\sum_\tau\frac{\tanh(\beta\xi_{k'\tau})}{2\xi_{k'\tau}}\right)\Delta^{\tau_3\tau_4}_{k'}, \quad (2)$$

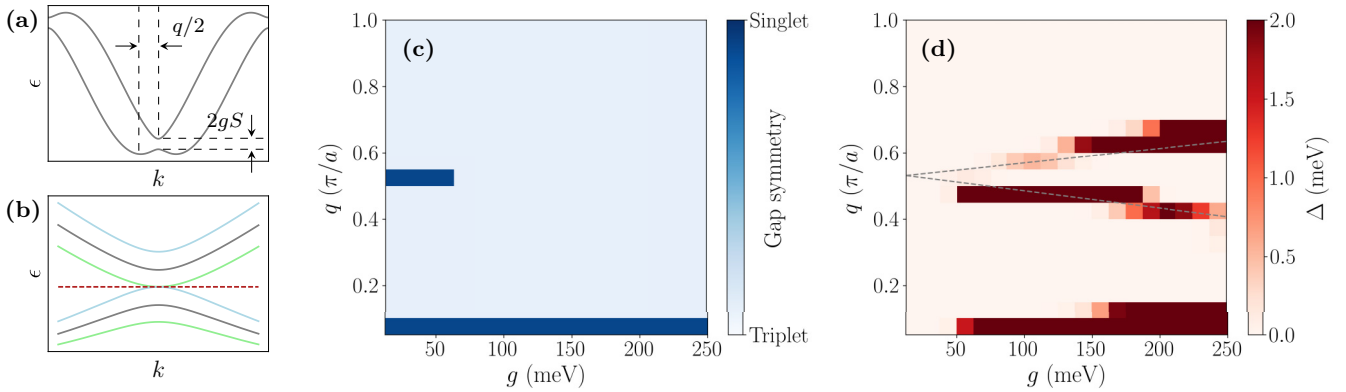

FIG. 2. Parameter dependence of magnon-mediated superconductivity. (a) Electronic band structure for a spin-electron coupling $g = 150$ meV and a spiral momentum $q = \pi/3a$. (b) Electronic band structure around $k = 0$ for a spin-electron coupling $g = 150$ meV and spiral momenta $q = 0.44\pi/a$ (green), $q = 0.5\pi/a$ (gray), and $q = 0.57\pi/a$ (blue). The red-dashed line indicates the chemical potential $\mu = -1.4$ eV. (c) Symmetry of the dominant superconducting gap as a function of spin-electron coupling g and spiral momentum q, for a chemical potential $\mu = -1.4$ eV. (d) Magnitude of the dominant superconducting gap as a function of spin-electron coupling g and spiral momentum q, for a chemical potential $\mu = -1.4$ eV. The gray-dashed lines indicate the positions of the van Hove singularities. In all panels the spin length is $S = 1$, the electronic hopping is $t = 1$ eV, and the exchange interaction is $J = 10$ meV.

where $\beta = 1/(k_B T)$ is the inverse temperature, and $\xi_k = \epsilon_k - \mu$. The gap equation can be viewed as an eigenvalue problem for the susceptibility matrix $\chi^{\tau_3\tau_4}_{\tau_1\tau_2}(k, k')$, implicitly defined by the right-hand side of Eq. (2), and superconductivity is signaled by the largest eigenvalue of this matrix exceeding unity [49].

On the mean-field level the electronic Hamiltonian is of the Bogoliubov-de Gennes (BdG) form, and can be written as $H = \sum_k \Phi_k^\dagger \mathcal{H}_k \Phi_k$ with $\mathcal{H}_k$ as a 4×4 matrix (see the SM [46]). The gap $\Delta_{\tau\tau'}$ can be decomposed into four components, given by the singlet gap $\Delta_s = (\Delta_{du} - \Delta_{ud})/2$ and the triplet gaps $\Delta_u = \Delta_{uu}$, $\Delta_d = \Delta_{dd}$, and $\Delta_p = (\Delta_{du} + \Delta_{ud})/2$. The subscripts u and d refer to the band index τ, which can be viewed as an effective spin index, where u (d) denotes the upper (lower) band or effective spin up (down). Due to the fermionic nature of the electronic operators, the singlet and triplet gaps are even and odd functions of k, respectively.

We begin with analyzing how the symmetry of the dominant superconducting gap depends on the spiral momentum q, the spin-electron coupling g, and the chemical potential μ. For parameters such that the energy difference $\epsilon_u(k_{Fu}) - \epsilon_d(k_{Fd}) \gg \Omega$, with $k_{F\tau}$ the Fermi momentum in band τ, and Ω a typical magnon energy, Cooper pairs will predominantly form from states within the same band. In this regime, the gap function becomes diagonal in the band indexes. At temperatures below 10 K, the pairing interaction is highly restricted to the Fermi surface, which for a 1D system consists of the points $\pm k_{F\tau}$. Restricting the gap equation to the Fermi surface, and neglecting contributions from interband scattering, Eq. (2) reduces to a 2×2 matrix problem and can be solved analytically (see the SM [46]). The eigenvalues of the susceptibility matrix are $\lambda_s = \chi(k_F, k_F) + \chi(k_F, -k_F)$ and $\lambda_p = \chi(k_F, k_F) - \chi(k_F, -k_F)$, for singlet and triplet pairing, respectively. These solutions show that the sign of the term $\chi(k_F, -k_F)$, accounting for scattering between the points k_F and $-k_F$, determines the symmetry of the dominant gap. Since only triplet pairing is consistent with the symmetry of intraband Cooper pairs, a consistent superconducting solution requires $\lambda_p > \lambda_s$. When $\epsilon_u(k_{Fu}) - \epsilon_d(k_{Fd}) \lesssim \Omega$, interband scattering becomes important, and the dominant superconducting gap is expected to have s-wave symmetry.

This qualitative analysis is in good agreement with the numerical solution of Eq. (2), showing that the dominant superconducting gap has triplet symmetry over a large fraction of the phase diagram [see Fig. 2(c)]. Only in regions where $\epsilon_u(k_{Fu}) - \epsilon_d(k_{Fd}) \lesssim \Omega$, such as close to the ferromagnetic limit $q = 0$, or when both $k_{F\tau}$ are close to the band edges (around $k_{F\tau} = 0$), does the dominant gap have singlet symmetry. In the strict ferromagnetic limit, this result can be established analytically (see the SM [46]), by noting that ferromagnetic magnons only scatter electrons with opposite spins. That such a large portion of the phase diagram is dominated by triplet pairing follows from the fact that singlet pairing requires interband scattering. For $k_{Fd} \neq k_{Fu}$, such scattering results in Cooper pairs with a finite center-of-mass momentum $k_{Fu} - k_{Fd} \sim q$, which strongly suppresses singlet pairing at finite q [50]. With increasing q, intraband magnon scattering therefore quickly becomes the dominant pairing mechanism, resulting in a gap with triplet symmetry. We note that in the antiferromagnetic limit $q = \pi$, an effective gap opens between the electronic bands, and only triplet pairing is possible.

We now analyze how the magnitude of the dominant superconducting gap depends on the magnetic parameters. In the regime $\epsilon_u(k_{Fu}) - \epsilon_d(k_{Fd}) \gg \Omega$, where interband scattering can be neglected, the zero temperature mean-field gap is given by $\Delta = 2\Omega e^{-1/(\rho_F U)}$ (see the SM [46]). Here ρ_F is the electronic density of states (DOS) at the Fermi level, and $U = U(k, k) - U(k, -k)$ the effective pairing interaction in the triplet sector. Since $U \sim g^2/\Omega$, the superconducting gap is expected to increase exponentially with the spin-electron coupling. To estimate Δ, we note that for an approximately linear dispersion, the electronic DOS tends to the constant $\rho_0 = 1/(4\pi t)$, while close to a band edge at energy ϵ_0 van Hove singularities of the form $\rho(\epsilon) = \rho_0\sqrt{t/(\epsilon - \epsilon_0)}$ develop. Approximating U with its value in the ferromagnetic limit,

$U = 4g^2S/\Omega$, the dimensionless coupling strength is $\lambda_{\text{eff}} = \rho_F U \approx g^2 S/(\pi t \Omega)$. For the typical values $S = 1$, $t = 1$ eV and $\Omega = 10$ meV, a spin-electron coupling of $g = 100$ meV gives a gap of $\Delta \sim 1$ meV, with significant enhancements expected at the van Hove singularities.

The magnitude of the superconducting gap is also obtained from a numerical solution of Eq. (2), whose largest eigenvalue λ is related to the gap by $\Delta = 2\Omega e^{-1/\lambda}$. The magnitude of Δ is shown in Fig. 2(d), and is found to generally increase with g as anticipated above. However, it also displays a clear nonmonotonic behavior with g, which can be attributed to the variation of the electronic DOS with the magnetic parameters. In particular, a gap between the upper and lower bands opens at $k = 0$ as a function of g, whose position varies with the spiral momentum q [see Fig. 2(b)]. For constant chemical potential, as assumed in Figs. 2(c) and 2(d), the DOS at the Fermi level therefore changes both with g and q, and is significantly enhanced at the van Hove singularities forming at the band edges. The diagonal lines in Fig. 2(d), emanating from $q \approx \pi/(2a)$, trace the van Hove singularities as a function of g. The overall magnitude of the gap, of order $\Delta \sim 1$ meV, is in line with the estimate above.

We now investigate the topological phases of the superconducting wire. In the effective single-band limit, where the chemical potential lies inside the band gap, the BdG Hamiltonian maps directly onto the Hamiltonian of the Kitaev chain [44]. This system is known to permit a topologically nontrivial phase with unpaired Majorana bound states appearing at each end of the quantum wire. Since the effective single-band limit of the model discussed here can be connected to the Kitaev model by continuously deforming the dispersion and gap function, its topological phase diagram is identical to the Kitaev model [26] (also see the SM [46]). It can be constructed by counting the number of intersections N between a line at constant chemical potential and the dispersion, with the topological index given by $\mathbb{Z}_2 = (N/2) \mod 2$.

To obtain the topological phase diagram of the full two-band model, we first consider the case where $\Delta_u \neq 0$ and $\Delta_d \neq 0$ but $\Delta_s = \Delta_p = 0$. In this limit, the model corresponds to two independent copies of the Kitaev model, and a $\mathbb{Z}_2$ invariant can be defined separately for each band. Denoting these invariants by Z_d and Z_u, the $\mathbb{Z}_2$ index of the full system is given by $Z_d Z_u$. Since adding finite interband pairings cannot close the superconducting gap, the full two-band model is continuously connected to the $\Delta_s = \Delta_p = 0$ limit, and for $\Delta_u \neq 0$ and $\Delta_d \neq 0$ the phase diagram can be constructed by counting the number of times N a line at constant chemical potential crosses the bands $\epsilon_{k\tau}$ [with $\mathbb{Z}_2 = (N/2) \mod 2$, see Fig. 3]. For $g = 0$ the system is always in a trivial regime, while for $g \neq 0$ two regions with nontrivial topology grow out of the upper and lower band edges. The size of these regions increase linearly with the magnitude of g. We note that in the antiferromagnetic limit the system is always in the trivial phase, since there is no effective single-band regime in this case.

Our results demonstrate that topological superconductivity is stabilized whenever the quantum wire is in an effective single-band regime. Such a regime can be experimentally realized by placing the chemical potential inside the $k = 0$ or $k = \pm\pi/a$ band gap Δ_b, induced by the coupling to the spiral. Magnon scattering further opens a superconducting gap Δ, whose magnitude is shown in Fig. 2(c) and is approximately determined by the product $g^2\rho_F/\Omega$. To favor topological superconductivity, it is desirable to find a system with a large g and ρ_F, but a small Ω (however, not too small, since Ω sets the upper limit of Δ).

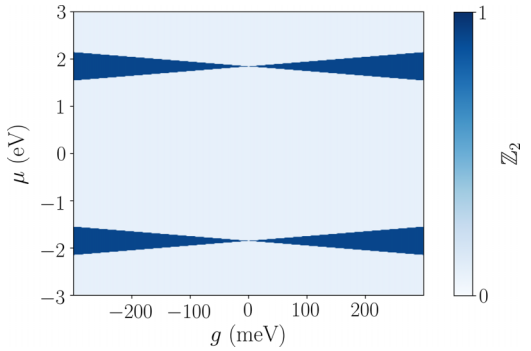

FIG. 3. Topological phase diagram of magnon-mediated superconductivity as a function of spin-electron coupling g and chemical potential μ. The magnetic spiral has a wave length $L = 8$ and momentum $q = \pi/(4a)$. The light regions show the trivial phase, while the dark regions correspond to a topological phase. The spin length is $S = 1$ and the electronic hopping $t = 1$ eV.

To realize the model of Eq. (1), several strategies are possible. The most straightforward is to consider a quantum wire in proximity to a helical magnet, as illustrated in Fig. 1. In this case, the wire could consist either of a simple metal, or a lightly doped or gate tuned semiconductor (such as InAs [51,52]), with a single active and largely uncorrelated band. For the helical magnet, it is preferable to use a material with a short spiral wave length ($\lambda \sim 10$ nm), low magnon energy, and large spin length, such as MnGe, MnSi or NiI_2 [53,54]. To maximize g, it is desirable to use a wire geometry where as much as possible of the wire is strongly coupled to the magnet. Estimating g for a general interface is hard, but based on earlier studies it is expected that $g \sim 10 - 100$ meV can be achieved [55–58]. An alternative strategy is to consider a quasi-one-dimensional multiband system [59,60], where the magnetic order and itinerant electrons coexist within the same material. In this case the spin-electron coupling is effectively the Hund's coupling J, potentially leading to large effective g on the order of 1 eV. However, since such multiband systems are typically strongly correlated, Eq. (1) should in this case be supplemented with additional interaction terms.

We have demonstrated that magnon fluctuations of a helical magnet can mediate triplet superconductivity in a proximate quantum wire. As the induced band gap and superconducting gap both increase with the spin-electron coupling g, various material engineering techniques such as wire geometry optimization, microstructuring, or cavity-enhanced light-matter couplings can be employed to maximize its value [51,61–64]. We expect that, utilizing such strategies, an effective coupling exceeding $g \approx 50$ meV can be achieved, allowing our protocol to surpass present state-of-the-art experiments with a topological superconducting gap of the order $\Delta \sim 0.1$ meV [39]. Compared to the

conventional scheme of generating 1D topological superconductivity combining proximity-induced superconductivity with large Rashba spin-orbit coupling and external magnetic fields, the main advantage of our proposal is the absence of fine tuning conditions.

The present model is a simplified description of a real quantum wire, and in reality effects coming from repulsive electron-electron interactions, disorder, and a more complex band structure should be included [65]. While the former is expected to compete with the magnon-mediated attraction, the later could result in a larger DOS at the Fermi level, thereby enhancing superconductivity. Another route to connect the present model with more realistic experimental setups is through the study of the corresponding system with open boundary conditions. In conclusion, our results identify quantum wires in proximity to noncollinear magnets as a promising platform to explore topological superconductivity in 1D.

We acknowledge fruitful discussions with Oladunjoye A. Awoga. F.V.B. acknowledges funding from the Swedish Research Council (VR), and E.V.B. acknowledges funding from the European Union's Horizon Europe research and innovation programme under the Marie Skłodowska-Curie Grant Agreement No. 101106809.

[1] J. Bardeen, L. N. Cooper, and J. R. Schrieffer, Theory of superconductivity, Phys. Rev. **108**, 1175 (1957).

[2] W. Eerenstein, N. D. Mathur, and J. F. Scott, Multiferroic and magnetoelectric materials, Nature (London) **442**, 759 (2006).

[3] X. Li, T. Qiu, J. Zhang, E. Baldini, J. Lu, A. M. Rappe, and K. A. Nelson, Terahertz field-induced ferroelectricity in quantum paraelectric $SrTiO_3$, Science **364**, 1079 (2019).

[4] D. Werdehausen, T. Takayama, M. Höppner, G. Albrecht, A. W. Rost, Y. Lu, D. Manske, H. Takagi, and S. Kaiser, Coherent order parameter oscillations in the ground state of the excitonic insulator Ta_2NiSe_5, Sci. Adv. **4**, eaap8652 (2018).

[5] G. Mazza, M. Rösner, L. Windgätter, S. Latini, H. Hübener, A. J. Millis, A. Rubio, and A. Georges, Nature of symmetry breaking at the excitonic insulator transition: Ta_2NiSe_5, Phys. Rev. Lett. **124**, 197601 (2020).

[6] R. B. Laughlin, Anomalous quantum Hall effect: An incompressible quantum fluid with fractionally charged excitations, Phys. Rev. Lett. **50**, 1395 (1983).

[7] X. G. Wen and Q. Niu, Ground-state degeneracy of the fractional quantum Hall states in the presence of a random potential and on high-genus Riemann surfaces, Phys. Rev. B **41**, 9377 (1990).

[8] A. Yu. Kitaev, Fault-tolerant quantum computation by anyons, Ann. Phys. (NY) **303**, 2 (2003).

[9] C. Nayak, S. H. Simon, A. Stern, M. Freedman, and S. Das Sarma, Non-Abelian anyons and topological quantum computation, Rev. Mod. Phys. **80**, 1083 (2008).

[10] D. Arovas, J. R. Schrieffer, and F. Wilczek, Fractional statistics and the quantum Hall effect, Phys. Rev. Lett. **53**, 722 (1984).

[11] A. Kitaev, Anyons in an exactly solved model and beyond, Ann. Phys. (NY) **321**, 2 (2006).

[12] L. Savary and L. Balents, Quantum spin liquids: A review, Rep. Prog. Phys. **80**, 016502 (2017).

[13] H. Bartolomei, M. Kumar, R. Bisognin, A. Marguerite, J.-M. Berroir, E. Bocquillon, B. Plaçais, A. Cavanna, Q. Dong, U. Gennser *et al.*, Fractional statistics in anyon collisions, Science **368**, 173 (2020).

[14] J. Nakamura, S. Liang, G. C. Gardner, and M. J. Manfra, Direct observation of anyonic braiding statistics, Nat. Phys. **16**, 931 (2020).

[15] J. M. Leinaas and J. Myrheim, On the theory of identical particles, Il Nuovo Cim. B **37**, 1 (1977).

[16] F. Wilczek, Quantum mechanics of fractional-spin particles, Phys. Rev. Lett. **49**, 957 (1982).

[17] L. Fu and C. L. Kane, Superconducting proximity effect and Majorana fermions at the surface of a topological insulator, Phys. Rev. Lett. **100**, 096407 (2008).

[18] S. Nakosai, Y. Tanaka, and N. Nagaosa, Two-dimensional *p*-wave superconducting states with magnetic moments on a conventional *s*-wave superconductor, Phys. Rev. B **88**, 180503(R) (2013).

[19] H.-H. Sun, K.-W. Zhang, L.-H. Hu, C. Li, G.-Y. Wang, H.-Y. Ma, Z.-A. Xu, C.-L. Gao, D.-D. Guan, Y.-Y. Li, C. Liu, D. Qian, Y. Zhou, L. Fu, S.-C. Li, F.-C. Zhang, and J.-F. Jia, Majorana zero mode detected with spin selective Andreev reflection in the vortex of a topological superconductor, Phys. Rev. Lett. **116**, 257003 (2016).

[20] G. C. Ménard, S. Guissart, C. Brun, R. T. Leriche, M. Trif, F. Debontridder, D. Demaille, D. Roditchev, P. Simon, and T. Cren, Two-dimensional topological superconductivity in Pb/Co/Si(111), Nat. Commun. **8**, 2040 (2017).

[21] A. Palacio-Morales, E. Mascot, S. Cocklin, H. Kim, S. Rachel, D. K. Morr, and R. Wiesendanger, Atomic-scale interface engineering of Majorana edge modes in a 2D magnet-superconductor hybrid system, Sci. Adv. **5**, eaav6600 (2019).

[22] Z. Wang, J. O. Rodriguez, L. Jiao, S. Howard, M. Graham, G. D. Gu, T. L. Hughes, D. K. Morr, and V. Madhavan, Evidence for dispersing 1D Majorana channels in an iron-based superconductor, Science **367**, 104 (2020).

[23] S. Kezilebieke, M. N. Huda, V. Vaňo, M. Aapro, S. C. Ganguli, O. J. Silveira, S. Głodzik, A. S. Foster, T. Ojanen, and P. Liljeroth, Topological superconductivity in a van der Waals heterostructure, Nature (London) **588**, 424 (2020).

[24] K. Flensberg, Tunneling characteristics of a chain of Majorana bound states, Phys. Rev. B **82**, 180516(R) (2010).

[25] Y. Oreg, G. Refael, and F. von Oppen, Helical liquids and Majorana bound states in quantum wires, Phys. Rev. Lett. **105**, 177002 (2010).

[26] R. M. Lutchyn, J. D. Sau, and S. Das Sarma, Majorana fermions and a topological phase transition in semiconductor-superconductor heterostructures, Phys. Rev. Lett. **105**, 077001 (2010).

[27] R. M. Lutchyn, E. P. A. M. Bakkers, L. P. Kouwenhoven, P. Krogstrup, C. M. Marcus, and Y. Oreg, Majorana zero modes in superconductor-semiconductor heterostructures, Nat. Rev. Mater. **3**, 52 (2018).

[28] K. T. Law, P. A. Lee, and T. K. Ng, Majorana fermion induced resonant Andreev reflection, Phys. Rev. Lett. **103**, 237001 (2009).

[29] T. D. Stanescu, R. M. Lutchyn, and S. Das Sarma, Majorana fermions in semiconductor nanowires, Phys. Rev. B **84**, 144522 (2011).

[30] J. Alicea, Y. Oreg, G. Refael, F. von Oppen, and M. P. A. Fisher, Non-Abelian statistics and topological quantum information processing in 1D wire networks, Nat. Phys. **7**, 412 (2011).

[31] V. Mourik, K. Zuo, S. M. Frolov, S. R. Plissard, E. P. A. M. Bakkers, and L. P. Kouwenhoven, Signatures of Majorana fermions in hybrid superconductor-semiconductor nanowire devices, Science **336**, 1003 (2012).

[32] A. Das, Y. Ronen, Y. Most, Y. Oreg, M. Heiblum, and H. Shtrikman, Zero-bias peaks and splitting in an Al-InAs nanowire topological superconductor as a signature of Majorana fermions, Nat. Phys. **8**, 887 (2012).

[33] A. D. K. Finck, D. J. Van Harlingen, P. K. Mohseni, K. Jung, and X. Li, Anomalous modulation of a zero-bias peak in a hybrid nanowire-superconductor device, Phys. Rev. Lett. **110**, 126406 (2013).

[34] S. M. Albrecht, A. P. Higginbotham, M. Madsen, F. Kuemmeth, T. S. Jespersen, J. Nygård, P. Krogstrup, and C. M. Marcus, Exponential protection of zero modes in Majorana islands, Nature (London) **531**, 206 (2016).

[35] M. T. Deng, S. Vaitiekėnas, E. B. Hansen, J. Danon, M. Leijnse, K. Flensberg, J. Nygård, P. Krogstrup, and C. M. Marcus, Majorana bound state in a coupled quantum-dot hybrid-nanowire system, Science **354**, 1557 (2016).

[36] F. Nichele, A. C. C. Drachmann, A. M. Whiticar, E. C. T. O'Farrell, H. J. Suominen, A. Fornieri, T. Wang, G. C. Gardner, C. Thomas, A. T. Hatke, P. Krogstrup, M. J. Manfra, K. Flensberg, and C. M. Marcus, Scaling of Majorana zero-bias conductance peaks, Phys. Rev. Lett. **119**, 136803 (2017).

[37] H. Zhang, D. E. Liu, M. Wimmer, and L. P. Kouwenhoven, Next steps of quantum transport in Majorana nanowire devices, Nat. Commun. **10**, 5128 (2019).

[38] E. Prada, P. San-Jose, M. W. A. de Moor, A. Geresdi, E. J. H. Lee, J. Klinovaja, D. Loss, J. Nygård, R. Aguado, and L. P. Kouwenhoven, From Andreev to Majorana bound states in hybrid superconductor-semiconductor nanowires, Nat. Rev. Phys. **2**, 575 (2020).

[39] M. Aghaee *et al.* (Microsoft Quantum), InAs-Al hybrid devices passing the topological gap protocol, Phys. Rev. B **107**, 245423 (2023).

[40] K. Mæland and A. Sudbø, Quantum topological phase transitions in skyrmion crystals, Phys. Rev. Res. **4**, L032025 (2022).

[41] K. Mæland and A. Sudbø, Topological superconductivity mediated by skyrmionic magnons, Phys. Rev. Lett. **130**, 156002 (2023).

[42] K. Mæland, S. Abnar, J. Benestad, and A. Sudbø, Topological superconductivity mediated by magnons of helical magnetic states, Phys. Rev. B **108**, 224515 (2023).

[43] A. Altland and M. R. Zirnbauer, Nonstandard symmetry classes in mesoscopic normal-superconducting hybrid structures, Phys. Rev. B **55**, 1142 (1997).

[44] A. Y. Kitaev, Unpaired Majorana fermions in quantum wires, Phys.-Usp. **44**, 131 (2001).

[45] C.-K. Chiu, J. C. Y. Teo, A. P. Schnyder, and S. Ryu, Classification of topological quantum matter with symmetries, Rev. Mod. Phys. **88**, 035005 (2016).

[46] See Supplemental Material at http://link.aps.org/supplemental/10.1103/PhysRevResearch.6.L022042 for additional details on the diagonalization of the magnon and electron sub-systems, the derivation of the electron-magnon interaction, the derivation of the effective electron-electron interaction, the derivation of the gap equation, and an extended discussion of the $\mathbb{Z}_2$ topological invariant of the superconducting system.

[47] E. Viñas Boström, F. G. Eich, and A. Rubio, Magnon frequency renormalization by the electronic geometrical spin torque in itinerant magnets, arXiv:2112.06547.

[48] S. Nadj-Perge, I. K. Drozdov, B. A. Bernevig, and A. Yazdani, Proposal for realizing Majorana fermions in chains of magnetic atoms on a superconductor, Phys. Rev. B **88**, 020407(R) (2013).

[49] P. B. Allen and B. Mitrović, Theory of superconducting tc, in *Solid State Physics* (Elsevier, New York, 1983), pp. 1–92.

[50] F. Loder, A. P. Kampf, and T. Kopp, Superconducting state with a finite-momentum pairing mechanism in zero external magnetic field, Phys. Rev. B **81**, 020511(R) (2010).

[51] M. Nilsson, F. Viñas Boström, S. Lehmann, K. A. Dick, M. Leijnse, and C. Thelander, Tuning the two-electron hybridization and spin states in parallel-coupled InAs quantum dots, Phys. Rev. Lett. **121**, 156802 (2018).

[52] R. Debbarma, M. Aspegren, F. Viñas Boström, S. Lehmann, K. Dick, and C. Thelander, Josephson current via spin and orbital states of a tunable double quantum dot, Phys. Rev. B **106**, L180507 (2022).

[53] N. Nagaosa and Y. Tokura, Topological properties and dynamics of magnetic skyrmions, Nat. Nanotechnol. **8**, 899 (2013).

[54] Q. Song, C. A. Occhialini, E. Ergeçen, B. Ilyas, D. Amoroso, P. Barone, J. Kapeghian, K. Watanabe, T. Taniguchi, A. S. Botana, S. Picozzi, N. Gedik, and R. Comin, Evidence for a single-layer van der Waals multiferroic, Nature (London) **602**, 601 (2022).

[55] Z. Qiao, W. Ren, H. Chen, L. Bellaiche, Z. Zhang, A. H. MacDonald, and Q. Niu, Quantum anomalous Hall effect in graphene proximity coupled to an antiferromagnetic insulator, Phys. Rev. Lett. **112**, 116404 (2014).

[56] T. Norden, C. Zhao, P. Zhang, R. Sabirianov, A. Petrou, and H. Zeng, Giant valley splitting in monolayer WS_2 by magnetic proximity effect, Nat. Commun. **10**, 4163 (2019).

[57] K. Mæland, H. I. Røst, J. W. Wells, and A. Sudbø, Electron-magnon coupling and quasiparticle lifetimes on the surface of a topological insulator, Phys. Rev. B **104**, 125125 (2021).

[58] C. Cardoso, A. T. Costa, A. H. MacDonald, and J. Fernández-Rossier, Strong magnetic proximity effect in van der Waals heterostructures driven by direct hybridization, Phys. Rev. B **108**, 184423 (2023).

[59] J. Schlappa, K. Wohlfeld, K. J. Zhou, M. Mourigal, M. W. Haverkort, V. N. Strocov, L. Hozoi, C. Monney, S. Nishimoto, S. Singh *et al.*, Spin-orbital separation in the

quasi-one-dimensional Mott insulator Sr_2CuO_3, Nature (London) **485**, 82 (2012).

[60] D. M. Kennes, L. Xian, M. Claassen, and A. Rubio, One-dimensional flat bands in twisted bilayer germanium selenide, Nat. Commun. **11**, 1124 (2020).

[61] P. J. W. Moll, Focused ion beam microstructuring of quantum matter, Annu. Rev. Condens. Matter Phys. **9**, 147 (2018).

[62] M. A. Sentef, M. Ruggenthaler, and A. Rubio, Cavity quantum-electrodynamical polaritonically enhanced electron-phonon coupling and its influence on superconductivity, Sci. Adv. **4**, aau6969 (2018).

[63] E. Barrigón, M. Heurlin, Z. Bi, B. Monemar, and L. Samuelson, Synthesis and applications of III-V nanowires, Chem. Rev. **119**, 9170 (2019).

[64] E. Viñas Boström, A. Sriram, M. Claassen, and A. Rubio, Controlling the magnetic state of the proximate quantum spin liquid α-$RuCl_3$ with an optical cavity, npj Comput. Mater. **9**, 202 (2023).

[65] S. Das Sarma, In search of Majorana, Nat. Phys. **19**, 165 (2023).